

Novel algorithms for efficiently
accumulating, analysing and
visualising full-waveform LiDAR in
a volumetric representation with
applications to forestry

submitted by

Milto Miltiadou

for the degree of Doctor of Engineering

of the

University of Bath

Centre for Digital Entertainment

and of the

Plymouth Marine Laboratory

NERC Airborne Research Facility

April 2017

COPYRIGHT

Attention is drawn to the fact that copyright of this thesis rests with its author. This copy of the thesis has been supplied on the condition that anyone who consults it is understood to recognise that its copyright rests with its author and that no quotation from the thesis and no information derived from it may be published without the prior written consent of the author.

This thesis may be made available for consultation within the University Library and may be photocopied or lent to other libraries for the purposes of consultation.

Signature of Author

Milto Miltiadou

Abstract

no more than 300 words

NOTES:

Blue colour: additions according to Neill's feedback,

Purple colour: addition/corrections according to Mike's comments

Red colour: notes

Gray colour: text that is going to be modified

To be added on top

Abstract

This study focuses on enhancing the visualisations and classifications of forested areas using coincident full-waveform (fw) LiDAR data and hyperspectral images. The ultimate aim is use both datasets to derive information about forests and show the results on a 3D virtual, interactive environment. Influenced by Persson et al (2005), voxelisation is an integral part of this research. The intensity profile of each full-waveform pulse is accumulated into a voxel array, building up a 3D density volume. The correlation between multiple pulses into a voxel representation produces a more accurate representation, which confers greater noise resistance and it further opens up possibilities of vertical interpretation of the data. The 3D density volume is then aligned with the hyperspectral images using a 2D grid similar to Warren et al (2014) and both datasets are used in visualisations and classifications.

Previous work in visualising fw LiDAR has used transparent objects and point clouds, while the output of this system is a coloured 3D-polygon representation, showing well-separated structures such as individual trees and greenhouses. The 3D density volume, generated from the fw LiDAR data, is polygonised using functional representation of object (FReps) and the marching cubes algorithm (Pasko and Savchenko, 1994) (Lorensen and Cline, 1987). Further, an optimisation algorithm is introduced that uses integral volumes (Crow, 1984) to speed up the process of polygonising the volume. This optimisation approach not only works on non-manifold object, but also a speed up of up to 51% was achieved. The polygon representation is also textured by projecting the hyperspectral images into the mesh. In addition, the output is suitable for direct rendering with commodity 3D-accelerated hardware, allowing smooth visualisation.

In future work, the effects of combining both hyperspectral imagery and fw LiDAR in classifications and visualisations are examined. At first, two pixel wise classifiers, a support vector machine and a Bayesian probabilistic model, will be used for testing the effects of the combination in generating tree coverage maps. Higher accuracy classification results are expected when metrics from both datasets are used together. Regarding the visualisations, the differences of applying surface reconstruction versus direct volumetric rendering will be discussed and an ordered tree structure with integral sums of the node values will be used for speeding up the ray-tracing of direct volumetric rendering and improving memory management of aforementioned optimisation algorithm with integral volumes. Further, deferred rendering is suggested for testing the visual human perception of projecting multiple bands of the hyperspectral images on the FW LiDAR

polygon representations. At the end of this project the combination of the datasets will be used along with the watershed algorithm for tree segmentation, which is useful for measuring the stem density of a forest and for tree species classifications.

from EDE:

Firstly, a new and fast way of aligning the FW LiDAR with Remotely Sensed Images has been developed in DASOS and by generating tree coverage maps it was shown that the combination of those datasets confers better remote survey results. This work was presented at the 36th ISRSE International Conference.

Secondly, automated detection of dead trees in native Australian forests has a significant role in protecting animals, which live in those trees and are close to extinction. DASOS allow the generation of 3D signatures characterising dead trees. A comparison between the discrete and FW LiDAR is performed to demonstrate the increased survey accuracy obtained when the FW LiDAR are used.

Finally, the last application is for improving visualisations for foresters. Foresters have a great knowledge about forests and can derive a wealth of information directly from visualisations of the remotely sensed data. This reduces the travelling time and cost of getting into the forests. This research optimises visualisations by using the new FW LiDAR representations and a speed of up to 51% has been achieved.

FW LiDAR has great potentials in forestry and this research has already started to have an impact in the FW LiDAR community by making those huge datasets easier to handle. DASOS is now used at Interpine Group Ltd, a world leading Forestry Company in New Zealand and it has been tested from a PhD student at Bournemouth University who looks into estimating bird distribution in the New Forest. In the future, it is expected that DASOS will be widely used in remote forest surveys (i.e. estimating the commercial value of a forest and detecting infected trees at early stages for treatment).

Acknowledgements

Above all, I would like to express my great gratitude to my industrial supervisors Dr. Michael Grant who had supported me continuously during my research and gave me the freedom to create a project of my own interest.

Then, I would like to thanks Dr. Matthew Brown, who helped me during my first years of my studies by giving me valuable and informative feedback. He was always there to keep me working on the right track.

Equally important is my current supervisor Dr. Neil D.F. Campbell and he is not to be missed from the acknowledgements.

Furthermore, special thanks are given to Dr. Mark Warren, Dr. Darren Cosker, MSc Susana Gonzalez Aracil and Dr. Ross Hill who occasionally advised me during my studies.

It further worth giving credits to my data providers, the Natural Environment Research Council's Airborne Research Facility (NERC ARF) and Interpine Group Ltd.

Last but not least, I am extremely grateful to my funding organisations, the Centre for Digital Entertainment and Plymouth Marine Laboratory, who supported financially and consequently made this research possible.

Abbreviations and Glossary

AGC	Automatic Gain Controller
ALS	Airborne Laser Scanning
APL	Airborne Processing Library
ARF	Airborne Research Facility
CG	Computer Graphics
CHM	Canopy Height Model
CUDA	parallel computing platform available on nvidia graphic cards
DASOS	(δασος=forest in Greek), the open source software implemented for managing FW LiDAR data
DBH	Diameter at Breast Height
DEM	Digital Elevation Model
DTM	Digital Terrain Model (DTM)
FW	Full-Waveform
GB	Gigabyte
GPU	Graphics Processing Unit
LiDAR	Light Detection And Ranging
MRI	Magnetic Resonance Imaging
NASA	National Aeronautics and Space Administration
NDVI	Normalised Difference Vegetation Index
NERC	Natural Environment Research Council
NIR	Near-Infrared Region of the electromagnetic spectrum
QGIS	Quantum Geographic Information System
SIMD	Single Instruction, Multiple Data
TB	Terabyte
VIS	Visual Spectrum
VLR	Variable Length Records
WPDF	Waveform Packet Descriptor Format
UK	United Kingdom

Publications

DASOS-User Guide, M. Miltiadou, N.D.F Campbell, M. Brown, S.C. Aracil, M.A. Warren, D. Clewley, D.Cosker, and M. Grant, Full-waveform LiDAR workshop at Interpine Group Ltd, Rotorua NZ, 2016

Improving and Optimising Visualisations of full-waveform LiDAR data, M. Miltiadou, M. Brown, N.D.F Campbell, D. Cosker, M. Grant, *EuroGraphics UK, Computer Graphics & Visual Computing*, 2016

University of Bath Alignment of Hyperspectral Imagery and Full-Waveform LiDAR data for visualisation and classification purposes, M. Miltiadou, M. A. Warren, M. Grant, and M. Brown, *The International Archives of Photogrammetry, Remote Sensing and Spatial Information Sciences*, vol. 40, no. 7, p. 1257, 2015.

Reconstruction of a 3D Polygon Representation from Full-Wavefrom LiDAR data, M. Miltiadou, M. Grant, M. Brown, M. Warren, and E. Carolan,*RSPSoc Annual Conference, New Sensors for a Changing World*, 2014.

Awards

EDE and Ravenscroft Prize - Finalist: Selected as one of the five finalists for this is a prestigious prize that recognises the work of best postgraduate researchers.

Student Poster Competition at Silvilaser.

Conference Presentations

Remote Sensing Cyprus (RSCy) Conference, 2017 , Paphos, Cyprus - Oral Presentation

ForestSAT Conference,2016 , Santiago, Chile - Oral Presentation

Computer Graphics & Visual Computing (CGVC),2016, Bournemouth, United Kingdom - Poster Presentation

Silvilaser, 2015, La Grant Motte, France - Oral Presentation

International Symposium of Remote Sensing of the Environment (ISRSE), 2015, Berlin, German - Oral Presentation

Remote Sensing and Photogrammetry Society (RSPSoc) Conference, New Sensors for a Changing world , 2014, Aberystwyth, United Kingdom - Oral Presentation

Workshops

Full day workshop about FW LiDAR and DASOS at *Interpine Ltd Group*, 2016,
Rotorua, New Zealand

Demonstration of DASOS_v2 at the practical LiDAR session at *the NERC ARF annual workshop*, 2017, Plymouth, United Kingdom

Contents

Abstract	i
Acknowledgements	iii
Abbreviations and Glossary	iv
Publications	v
Awards	v
Conference Presentations	v
Workshops	vi
List of Figures	ix
1 Introduction	1
1.1 Forest Monitoring: Importance and Applications	1
1.2 Background Information about Remote Sensing and Airborne Laser Scan- ning Systems	1
2 Acquire Data	2
3 Overview of Thesis	3
4 The open source software DASOS and the Voxelisation Approach	4
5 Surface Reconstruction from Voxelised FW LiDAR Data	5
6 Optimisation Attempts for the Surface Reconstruction	6
7 Alignment with Hyperspectral Imagery	7
8 Detection of Dead Standing Eucalyptus For Managing Biodiversity in Native Australian Forest	8
8.1 Introduction	8
8.2 Materials	12

8.3	Methods and Algorithms / Statistical Analysis	16
8.4	Evaluation	24
8.5	Discussion	24
8.6	Future Work	25
9	Overall Results	26
10	Conclusions	27
10.1	Contributions	28
	Bibliography	28
	A DASOS user guide	i
	B Case Study: Field Work in New Forest	ii

List of Figures

8-1	Animals Closes to Extinction	10
8-2	LiDAR point cloud showing that there are very limited points reflected from tree trunks.	11
8-3	The study area is depicted by green ($542km^2$), the yellow strips are the LiDAR flightlines and the red dots are the position of the field plots. <i>**Note: this image many need to be removed due to confidentiality of the company. I will talk with them and hopefully it will be ok.</i>	13
8-4	Structure of Red Gum Forest in south-eastern Australia.	14
8-5	Example of dead trees indicating their variance in shape.	14
8-6	Example of a dead tree in relation to the discrete LiDAR point cloud.	15
8-7	Parameters used in Quick TERRain Modeller to obtain the DTM used here.	17
8-8	Showing the difference in the DEM before and after subtracting the terrain height. It is clearly shown that the ground in the right image is flat.	17
8-9	This figure shows what priors were created for testing and how they are divided for cross validation.	18
8-10	22
8-11	23
8-12	24

Chapter 1

Introduction

- 1.1 Forest Monitoring: Importance and Applications
- 1.2 Background Information about Remote Sensing and Airborne Laser Scanning Systems

Chapter 2

Acquire Data

Chapter 3

Overview of Thesis

Chapter 4

The open source software DASOS and the Voxelisation Approach

Chapter 5

Surface Reconstruction from Voxelised FW LiDAR Data

Chapter 6

Optimisation Attempts for the Surface Reconstruction

Chapter 7

Alignment with Hyperspectral Imagery

Chapter 8

Detection of Dead Standing Eucalyptus For Managing Biodiversity in Native Australian Forest

8.1 Introduction

8.1.1 The Importance of Dead Wood

The value of dead trees from a biodiversity management perspective is large. Once a tree dies, its contribution to our ecosystem continues. The woody structure remains for centuries and it contributes to forest regeneration while providing resources for numerous surrounding organisms [71]. As an indication, more than 4000 species inhabit dead wood in Finland [72], where an estimate of 1000 species has been extinct [73]. These species do not only include animals and birds but also organisms, like fungi. Fungi contributes to wood decaying, formation of hollows and biodiversity, which is an important factor for a resilient ecosystem [74]. Observing the changes of fungal diversity on decaying wood has an increased interest in science [75] [76] [77] in order to ensure the continuous existence of decaying wood in forests.

** NEill comma where: Specifically, in Australia, tree

Specifically in Australia, tree hollows play a significant role in managing biodiversity. Nearly all arboreal mammals rely on hollows with the exception of the Koala and perhaps Ringtail Possums that preferentially make a stick nest, but they use hollows as well. Additionally, a large number of Australian bird species rely on hollows for shelters

[5]. Nevertheless, Australia has no real hollow creators unlike the northern hemisphere (e.g. Woodpeckers), and therefore it relies predominantly on natural processes of limb breakage, insect and fungal attack when access points are provided through damage caused by wind, storms and fire.

This kind of hollows take hundreds of years to form and because of that it is more likely to exist on dead trees. In Australia, studies predict shortage of hollows for colonisation in the near future [3] [4]. Therefore automated detection of them plays a significant role in protecting those animals. As an indicator of the importance of hollows in managing biodiversity, a list of a few of the species that rely on hollows was provided by the Forestry Corporation of NSW. Those species are shown at Figure 8-1. According to the Department of the Environment of Australian Government and the Government of Western Australia, six of them are protected, threatened or close to extinct [78] [79]. Figure 8-1 shows the species from the provided list and the six protected species have a red border and their names are bold in the description.

For the aforementioned reasons, monitoring dead trees is essential for having a resilient ecosystem. Nevertheless, the distribution of dead trees significantly varies making detection of them difficult [80]. Remote sensing approaches has been introduce to automate the process of monitoring forest and further increase the spatial resolution of the monitored area. The following section gives an overview of the related work undertaken in Remote Sensing.

8.1.2 Related Work

Remote Sensing was introduced for automatically detecting dead trees, because field-work is time consuming considering their variance spread and the size of the relevant forests. From a classification perceptive, the task of identifying dead standing and dead fallen trees is different. Fallen trees are identified by detecting segments or line-like features on the terrain surface using LiDAR data [81] [82]. Regarding standing dead trees, their shape (reduced number of leaves or broken branches) [83] and light reflectance (less green light illuminated) [84] are important factors for identifying them.

Previous work on dead standing trees detection performs single tree crown delineation before health assessment [83] [85]. Tree-crown delineation is usually done by detecting local maxima from the canopy height model (CHM) and then segmenting trees with watershed algorithm [86]. Improvements has been achieved by introducing markers controlled watershed [87] and structural elements of tree crowns with different sizes [88]. Additionally, Popescu and Zhao analyse the vertical distribution of the LiDAR points in conjunction with the local maximum filtering of CHM [89].

In the case of Eucalyptus, single tree detection is a challenge on its own, due to their



Figure 8-1: A number of species that rely on tree hollows of which the red ones / bold ones are close to extinction: Kookaburra, Sulphur Crested Cockatoo, **Corella**, Crimson Rosella, Eastern Rosella, Galah, Rainbow Lorikeet, Musk Lorikeet, Little Lorikeet , Red-winged Parrot, **Superb Parrot**, Cockatiel, Australian Ringneck (Parrot), Red-rumped Parrot, Powerful Owl, Sooty Owl, Barking Owl, **Masked Owl**, **Barn Owl**, White-throated Treecreeper, Hollow Owl, **Brush-tailed Possum** (mammal)¹

¹The images of the birds were taken from the following links (Retrieved on the 27th of April 2016): Kookaburra: <<http://tenrandomfacts.com/blue-winged-kookaburra/>>, Sulphur Crested Cockatoo: <<http://aussiegal7.deviantart.com/art/Sulphur-Crested-Cockatoo-08-153341893>>, Corella: <<http://www.theparrotplace.co.nz/all-about-parrots/long-billed-corella/>>, Superb Parrot: <<http://www.davidkphotography.com/?showimage=637>>, Crimson Rosella: <http://25.media.tumblr.com/tumblr_m3mo89c40r1r4t9h1o1_1280.jpg>, Eastern Rosella: <http://2.bp.blogspot.com/-pYxw51WjSOY/UB-LEFgd2KI/AAAAAAAAGw/9z60PUWE6TE/s1600/_GJS6601-as-Smart-Object-1.jpg>, Rainbow Lorikeet: <https://www.reddit.com/r/pics/comments/328fvc/a_rainbow_lorikeet_found_in_coastal_regions/>, Musk Lorikeet: <http://www.rymich.com/girraween/photos/animals/birds/medium/glossopsitta_concinna/glossopsitta_concinna_001.jpg>, Little Lorikeet: <<http://www.pbase.com/sjmurray/psittacidae>>, Red-winged Parrot: <<https://www.pinterest.com/pin/395894623469889727/>>, Cockatiel: <<http://up.parsipet.ir/uploads/Cockatiels-for-sale.jpg>>, Australian Ringneck (Parrot): <<http://ontheroadmagazine.com.au/wp-content/uploads/2015/09/Twenty-eight-parrot-2-min.jpg>>, Red-rumped Parrot: <<http://parrotfacts.net/wp-content/uploads/Red-Rumped-Parrot-on-a-tree.jpg>>, Powerful Owl: <http://farm1.staticflickr.com/219/495796536_f78dac04c1.jpg>, Sooty Owl: <http://www.mariewinn.com/marieblog/uploaded_images/screech2-738532.jpg>, Barking Owl: <<http://www.pcpimages.com/Nature-and-Wildlife/Birds/i-7JKSTp5/1/L/owl%20%281%20of%201%29-L.jpg>>, Masked Owl: <http://www.survival.org.au/images/birds/masked_owl_2_600.jpg>, Galah: <<https://www.pinterest.com/pin/537546905498955709/>>, White-throated Treecreeper: <<https://geoffpark.files.wordpress.com/2011/09/female-white-throated-treecreeper.jpg>>,

irregular structure and multiple trunk splits. In other words, each tree trunks splits create a local maximum leading into over-segmentation when tree crowns are detected by local maxima filtering. Shendryk published a eucalyptus delineation algorithm that starts segmentation from bottom to top. In this paper, the trunks point cloud is separated from the leaves and individual trunks are identified before proceeding to crown segmentation [90]. Nevertheless, for that project only 17 flightlines of LiDAR data were collected. The density resolution starts from 12 points/ m^2 and goes up to 36 points/ m^2 around forested areas. For small research projects capturing this high resolution is acceptable, but for commercial use and larger areas, the density of data collected is above the optimal resolution for a cost effective versus quality acquisition [91]. The project of this thesis is much larger. The resolution of our acquired LiDAR data has an average of four pulses per square meter, which is considered an optimal resolution in relation to the cost. But because of the tree height (up to 43m according to the fieldwork), a small amount of pulse intensity reached the trunks and the recorded waveform do not include enough information for individual trunk detection. An example of this project's discrete LiDAR data is shown in Figure 8-2 and the missing information about the trunks is depicted.

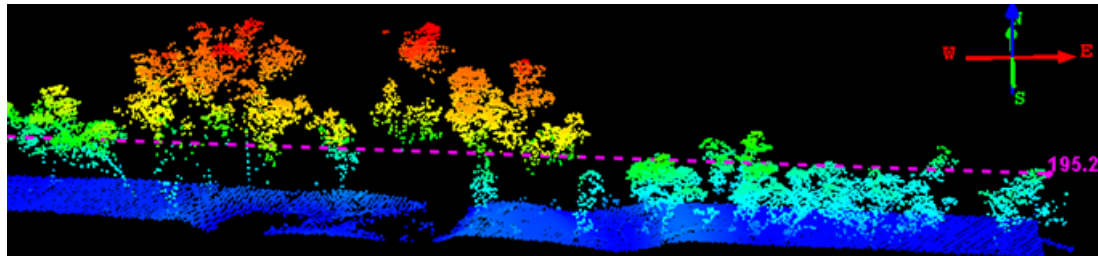


Figure 8-2: LiDAR point cloud showing that there are very limited points reflected from tree trunks.

*****Note read again to make sure it matches OK**

The acquired data are full-waveform LiDAR data. Traditional ways of interpreting FW LiDAR data, suggests extraction of a denser points cloud using Gaussian decomposition [29] [30]. Nevertheless, in this project we uses the open source software DASOS. DASOS was influenced by Persson et al, 2005, who used voxelisation to visualise the waveforms [26]. But, it does not only uses voxelisation for visualisations but also for extracting metrics useful in classification. It further normalises the intensities so that equal pulse length exists inside each voxel, making intensities more meaningful. It is further seems that the literature is moving towards voxelisation with promising results obtained at recent publication on tree species classification [33].

Hollow Owl: <http://www.mariewinn.com/marieblog/uploaded_images/screech2-738532.jpg>

Here, it is introduced an approach for quick dead tree detection derived from the boost cascade approach [92] but extended into 3D. This approach further contains similarities of the 3D tree shape signatures proposed by Dong, 2009, for distinguishing Oaks from Douglas fir tree crowns [93].

8.2 Materials

8.2.1 Study Area

The study area (Figure 8-3) is a native River Red Gum (*Eucalyptus camaldulensis*) forest of size 542km^2 in south-eastern Australia. The regeneration of the eucalyptus is extremely dependant in floods and therefore, their distribution in respect to density, health and age is highly variance [94]. Additionally, the height of *Eucalyptus camaldulensis* reaches up to $30 - 40\text{m}$ and their structural complexity is high with multiple trunk splits [95]. The size and structure of the forest, with a human as reference, is depicted in Figure 8-4, while examples of the variance shape of dead trees is shown in Figure 8-5.

8.2.2 Acquired full-waveform LiDAR data

Multiple-echo, full-waveform (FW) LiDAR data are supplied by RPS Australia East Pty Ltd. The data were acquired from 900m above ground level, using the Trimble AX60 Airborne LiDAR sensor, which was released in October 2013 [96]. The wavelength of the emitted laser was 1062nm, the maximum scan angle was 60 degrees, and the pulse rate was 400kHz. The acquisition was held from the 6th of March till the 31st of March 2015. The collected LiDAR were delivered into 206 flightlines, of which 13 are cross runs used for geometric correction. There is also a 30% of swath overlap. The point spacing along and across the track is 0.48m and the average point spacing is 4.3 points per square meter. Figure 8-6 shows an example of a dead tree in respect to the acquired discrete LiDAR point cloud. Detailed information about FW LiDAR related concepts are given in section 2.

8.2.3 Field Data

The field data were collected in July 2015 during the winter season of Australia and they include tree and canopy related measurements on circular plots. There are 33 plots with radius 35.68m and area 0.4ha allocated randomly inside the study area. On these plots, a total of 2386 trees were individually measured. Tree measurements include the geo-location, the trunk diameter at the standard height of 1.3m (breast height), height,

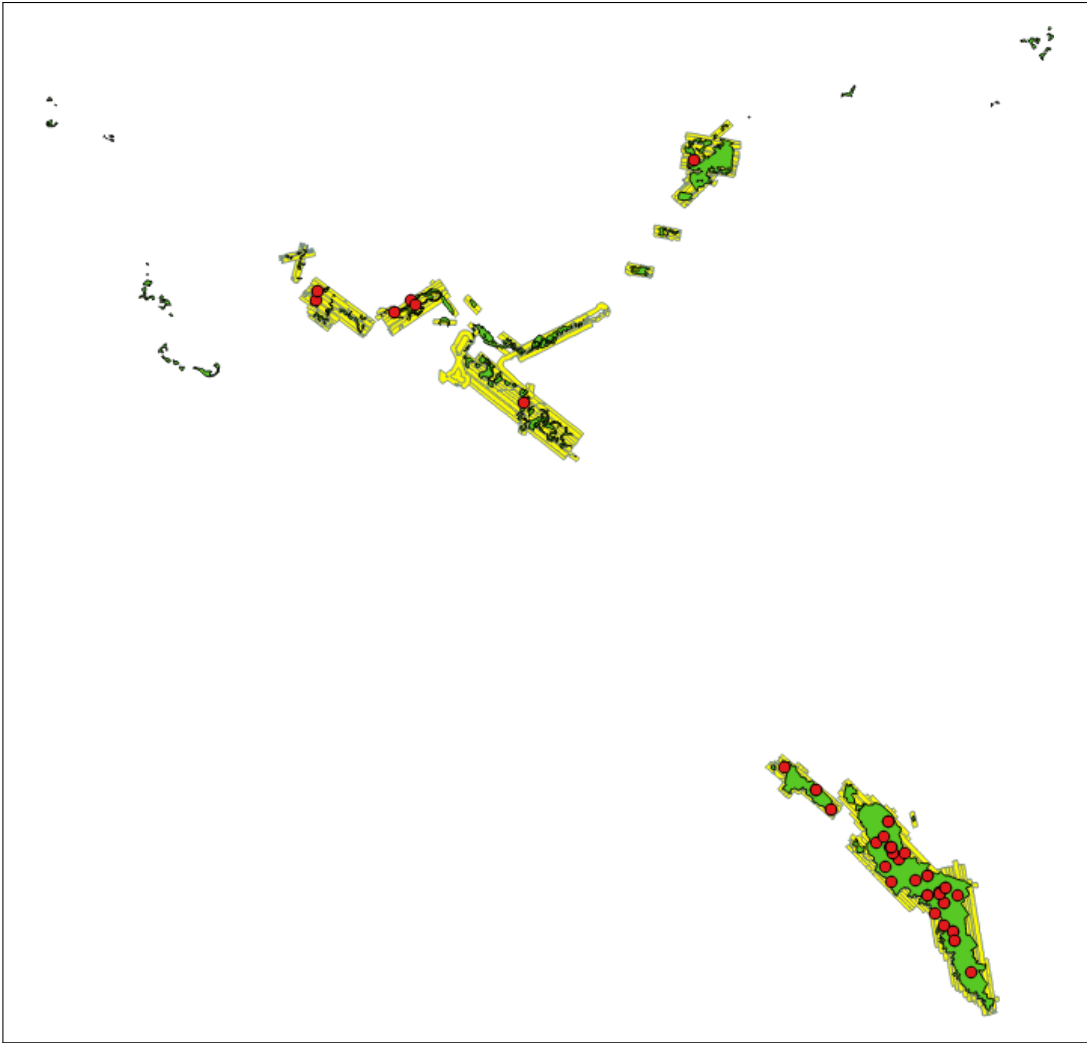


Figure 8-3: The study area is depicted by green (542km^2), the yellow strips are the LiDAR flightlines and the red dots are the position of the field plots. ****Note: this image many need to be removed due to confidentiality of the company. I will talk with them and hopefully it will be ok.**

species and health conditions (i.e. dead or alive). The geo-location of each tree is defined by the magnetic bearing from the centroid of the plot in degrees (range [1, 360]) and the distance from the centroid in meters. The northing and easting coordinates of the geo-location of each tree were calculated in post-processing.

Inside the field data, there are 260 dead trees recorded. Nevertheless, not all of those trees are considered useful for biodiversity. Dead trees with big Diameter at Breast Height (DBH) are more likely to contain hollows. Additionally, trees with DBH smaller than the footprint spacing of the LiDAR data are not identifiable from the FW



Figure 8-4: Structure of Red Gum Forest in south-eastern Australia.



Figure 8-5: Example of dead trees indicating their variance in shape.

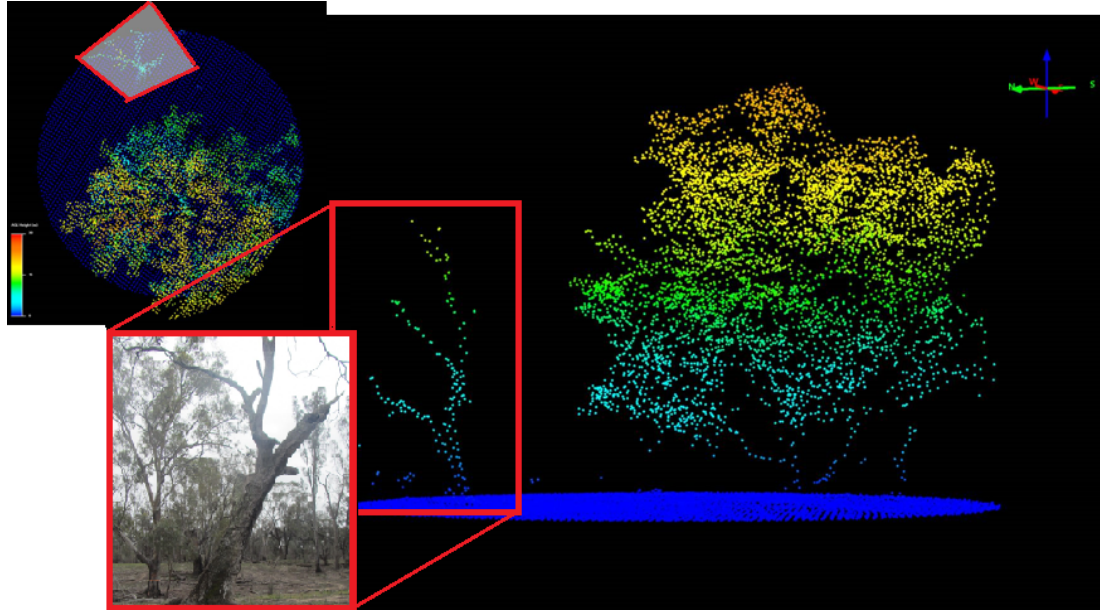


Figure 8-6: Example of a dead tree in relation to the discrete LiDAR point cloud.

LiDAR data. Table 8.1 shows the number of dead and alive trees in respect to their DBH.

DBH	Dead Trees	Alive Trees
>2000	0	1
1000-2000	7	21
600-1000	8	146
400-600	26	290
300-400	32	286
200-300	50	462
100-200	125	904
<100	11	16
Total	260	2126

Table 8.1: Number of trees according to their DBH. ****Note: I think it is in centimeter but I will confirm it with the company and add it afterwards.**

Please note that the aforementioned field data were provided by Forestry Corporation of NSW, Wauchope, Australia and Interpine Ltd Group, New Zealand. For this thesis, a case study for collecting field data was conducted in New Forest, UK. This helped to better understand classification challenges in forestry applications. More information about this study is provided in Appendix B.

8.2.4 Fieldplots Challenges

It worth mentioning the challenges of working with these fieldplots since they influences the quality of the classifier and the accuracy of the results.

1. A single tree may be recorded as multiple trees if there is a trunk split bellow the breast height of 1.3m. Furthermore, 91.59% are River Red Gum and the rest are Black Box (*Eucalyptus largiflorens*) and Wattle group (*Acacia* spp.).
2. Mention accuracy of data - add img of misplaced tree.

8.3 Methods and Algorithms / Statistical Analysis

steps

- Subtract DTM From full-waveform LiDAR
- DASOS and 3D priors
- Random Forest for identifying the most significant features
- Nearest Neighbour
- Thinning Algorithm
- Remove Ground and noisy columns using Gaussian decomposition
- Evaluation

8.3.1 Subtract DTM from FW LiDAR

DASOS has a feature for subtracting pre-calculated Digital Terrain Model (DTM) saved into .bil files. Generating DTM is beyond the scope of this research and the DTM files used, were provided by Interpine Ltd Group. The provided DTM files were generated using the Quick Terrain Modeller from the discrete LiDAR using the parameters shown in Figure 8-7.

The subtraction of the DTM is done during the voxelisation (Section 4). The terrain height is subtracted from the position of the sample and then inserted into the volume. Please note that this terrain value is not subtracted from the origin of each pulse but from the position of each sample since the terrain value at the origin and the terrain value at the position of the sample may differ. Figure 8-8 shows an example of a DEM generated before and after the subtraction using DASOS.

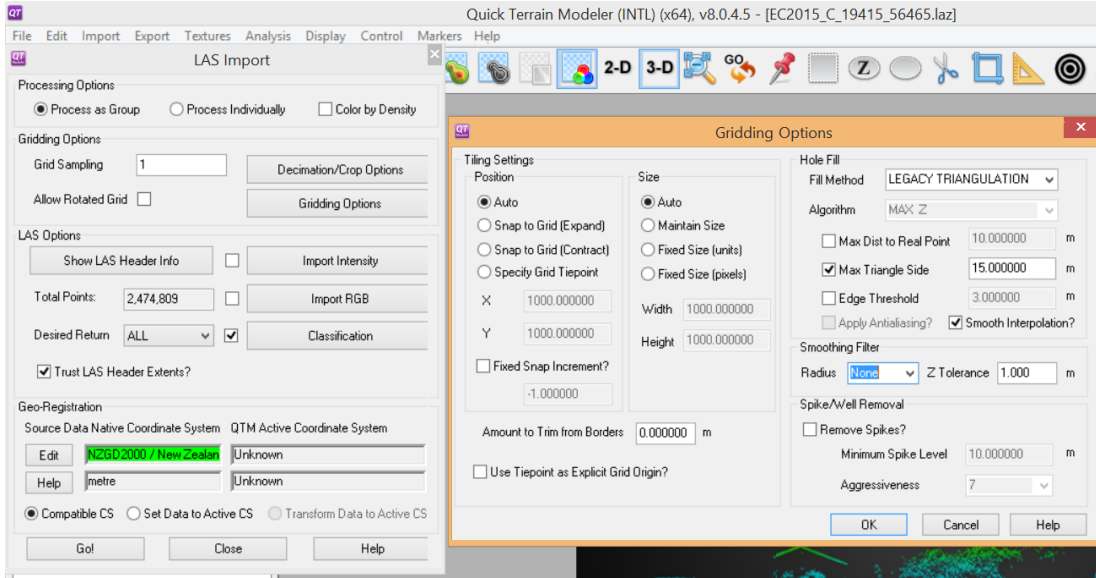


Figure 8-7: Parameters used in Quick TERRain Modeller to obtain the DTM used here.

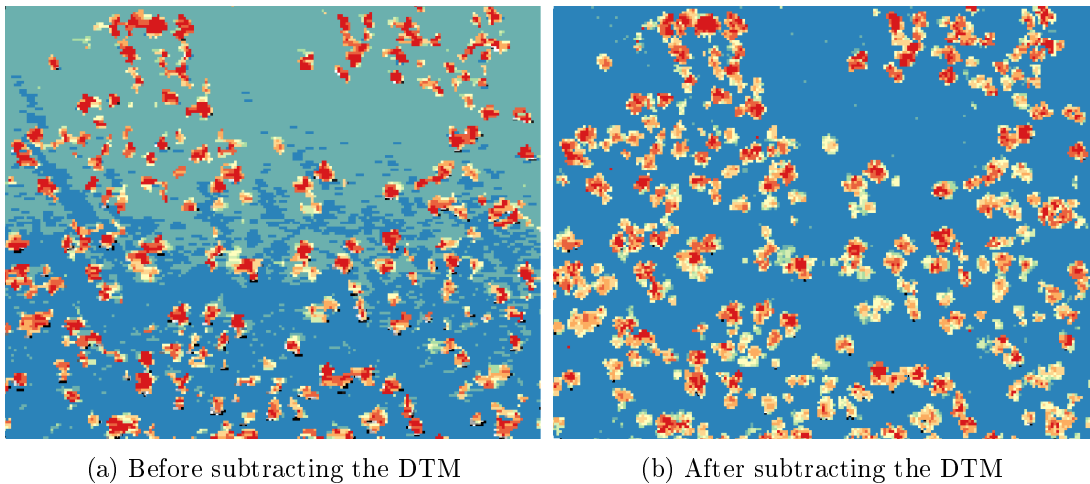


Figure 8-8: Showing the difference in the DEM before and after subtracting the terrain height. It is clearly shown that the ground in the right image is flat.

8.3.1.1 DASOS and 3D priors

Here, the 3rd feature of DASOS (Table ??) is used for generating 3D priors characterising dead standing Eucalypt trees. This section explains how this feature works and what the training/testing data were obtained using this feature of DASOS.

In a few words, the 3D priors contain local information of small areas within the voxelised FW LiDAR space.

The priors are exported into .csv files for easy manipulation into software packages

for statistical analysis like R and matlab. For example, a 3D prior could contain information about the shape of a dead tree. There are two options about the information exported and two options for the shape of the priors.

The 3D shape signatures were generated by getting the distance distribution of random LiDAR point pairs of the two tree crown classes: Oaks and Douglas [93]

Figure 8-9

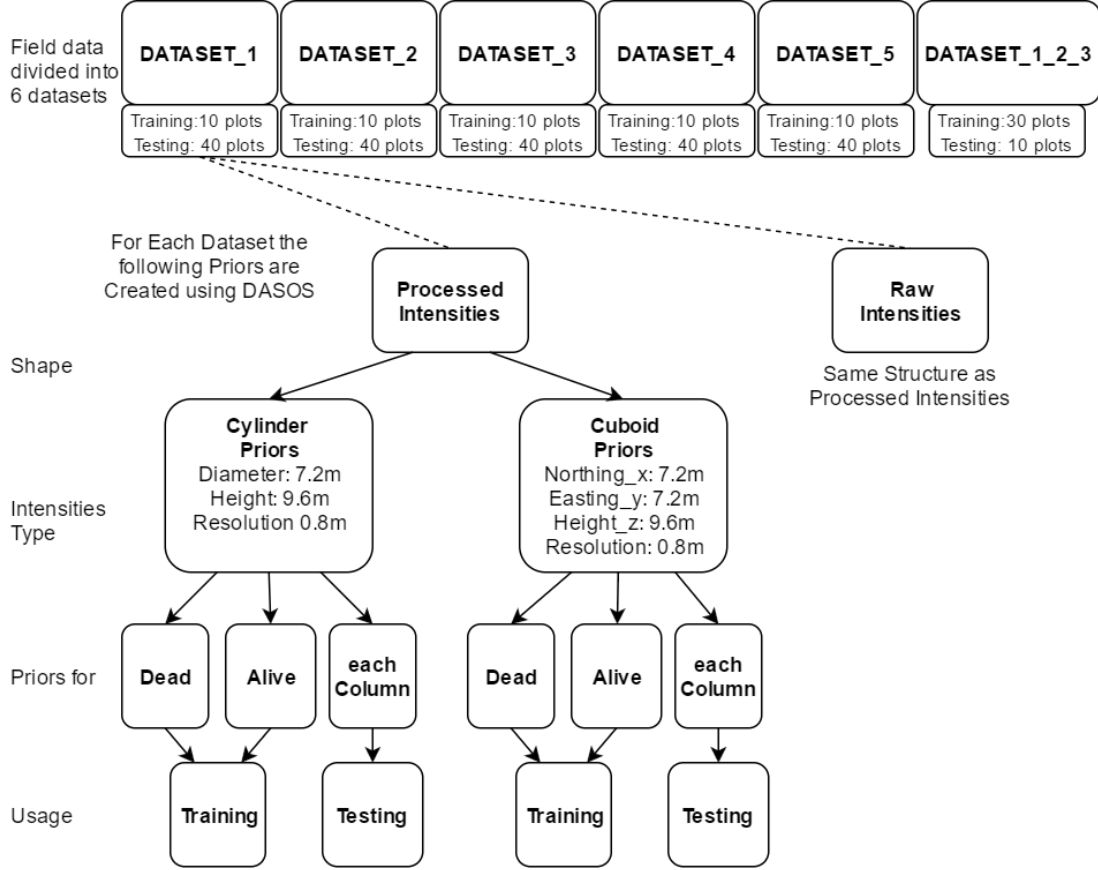


Figure 8-9: This figure shows what priors were created for testing and how they are divided for cross validation.

By the end it is worth mentioning that the dead tree detection is the first application of the 3D priors feature of DASOS, which was released on the 20th of January 2017 [97].

Explanation of the 3D priors Output with the Processed Intensities	
Label	Description
Height_Middle_Column	The height of the middle column of the prior
Height_Mean	The Mean height of all the columns included in the template
Height_Median	The Median height of all the columns included in the template
Height_Std	The Standard Deviation of the heights of the columns included in the template
Sum_Int_Diff_X	The Mirror Summed Difference of the intensities using the middle column in the x-axis as the axis of symmetry
Sum_Int_Diff_Y	The Mirror Summed Difference of the intensities using the middle column in the y-axis as the axis of symmetry
Sum_Int_Diff_Z	The Mirror Summed Difference of the intensities using the middle column in the z-axis as the axis of symmetry
Max_Int	The maximum intensity found inside the prior
Min_Int	The minimum intensity found inside the prior
Ave_Int	The average intensity of the voxels that contain an intensity above the isolevel
Median_Int	The median intensity of the voxels
Per_Int_Above_Iso	Percentage of voxels that contain an intensity above the isolevel
Dis_Mean	Mean distance from the central voxel to every voxel that contains an intensity above the isolevel
Dis_Median	Median distance from the central voxel to every voxel that contains an intensity above the isolevel
Dis_Std	The Standard Deviation of the distances between the central voxel and every voxel that contains an intensity above the isolevel
Top_Patch_Len_Middle_Col	The length of the top patch of the middle column of the prior

Top_Patch_Len_Mean	The Mean length of all the top patches
Top_Patch_Len_Median	The Median length of all the top patches
Top_Patch_Len_Std	The Standard Deviation of all the top patches
Mirror_Diff_X_Mean	The Mean Mirror Difference of the voxel intensities with the middle column of the x-axis as the symmetric axis
Mirror_Diff_X_Median	The Median Mirror Difference of the voxel intensities with the middle column of the x-axis as the symmetric axis
Mirror_Diff_X_Std	The Standard Deviation Mirror Difference of the voxel intensities with the middle column of the x-axis as the symmetric axis
Mirror_Diff_Y_Mean	The Mean Mirror Difference of the voxel intensities with the middle column of the y-axis as the symmetric axis
Mirror_Diff_Y_Median	The Median Mirror Difference of the voxel intensities with the middle column of the y-axis as the symmetric axis
Mirror_Diff_Y_Std	The Standard Deviation Mirror Difference of the voxel intensities with the middle column of the y-axis as the symmetric axis
Mirror_Diff_Z_Mean	The Mean Mirror Difference of the voxel intensities with the middle column of the z-axis as the symmetric axis
Mirror_Diff_Z_Median	The Median Mirror Difference of the voxel intensities with the middle column of the z-axis as the symmetric axis
Mirror_Diff_Z_Std	The Standard Deviation of the Mirror Difference of the voxel intensities with the middle column of the z-axis as the symmetric axis

Table 8.2: The three functionalities of DASOS

In the following section, the images and examples are taken from the Cylinder processed parameters but it done for all four test cases and cross validated using the 5 datasets division.

8.3.2 Random Forest

Images and examples for Cylinder processed parameters but it done for all four test cases and cross validated using the 5 datasets division.

Random Forest failed to find relation between the 3D priors with the Raw Intensities due to the irregular shapes of Eucalyptus trees and probably due to the scan from different angles. Raw Intensities may be useful for identifying pine trees in commercial forest, where the variance between each other is smaller.

Therefore from here we only test processed intensities with 3D cylindrical and 3D rectangular cuboid priors.

Identified the most significant features for detecting dead trees and then we build the following probabilistic model.

8.3.3 Probabilistic Model

We don't go straight to classification because in the testing data, we put a prior for each column and therefore many columns that contain dead trees are not marked correctly. And we wrote a probabilistic model using the most significant features identified by the random forest.

k-nearest neighbour: distance from the centre of mean for each of the first 5 significant features

$$P = P(\text{dead})/(P(\text{dead})+P(\text{alive}))$$

from that get grey scale field of the results

8.3.4 Ground Mask

threshold ground: Histogram of heights, because subtracted DTM,everything below 20 is considered ground.

Great histogram of the height map generated using the 2D metrics of DASOS.

Create three classes : ground, trees and noise

Because the DTM has been subtracted (Section 8.3.1), the ground is easily separated from the trees.

Mask out ground and noise

8.3.5 Filtering and Local Maxima

Salt and pepper filter

Smoothing filter

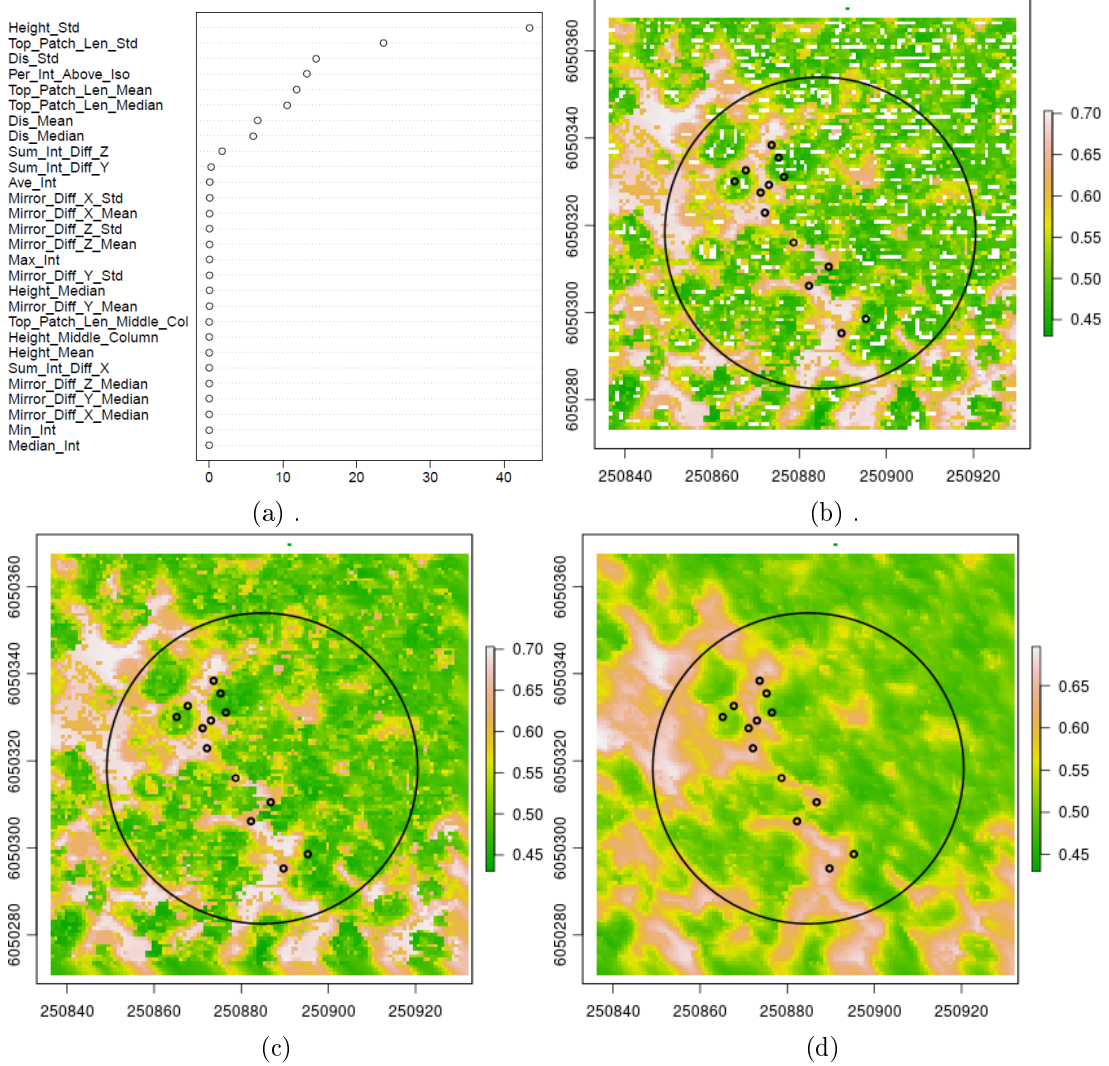


Figure 8-10

8.3.6 Threshold

if a local maxima is found but the probability of being a dead is low then it is not a dead tree. This is defined by a user defined constant threshold.

threshold values according to the probability of been a dead tree >0.62

8.3.7 Segmentation

remove pixels that have <3 neighbouring dead pixels and add those which have plenty around them

seed point growth segmentation algorithm

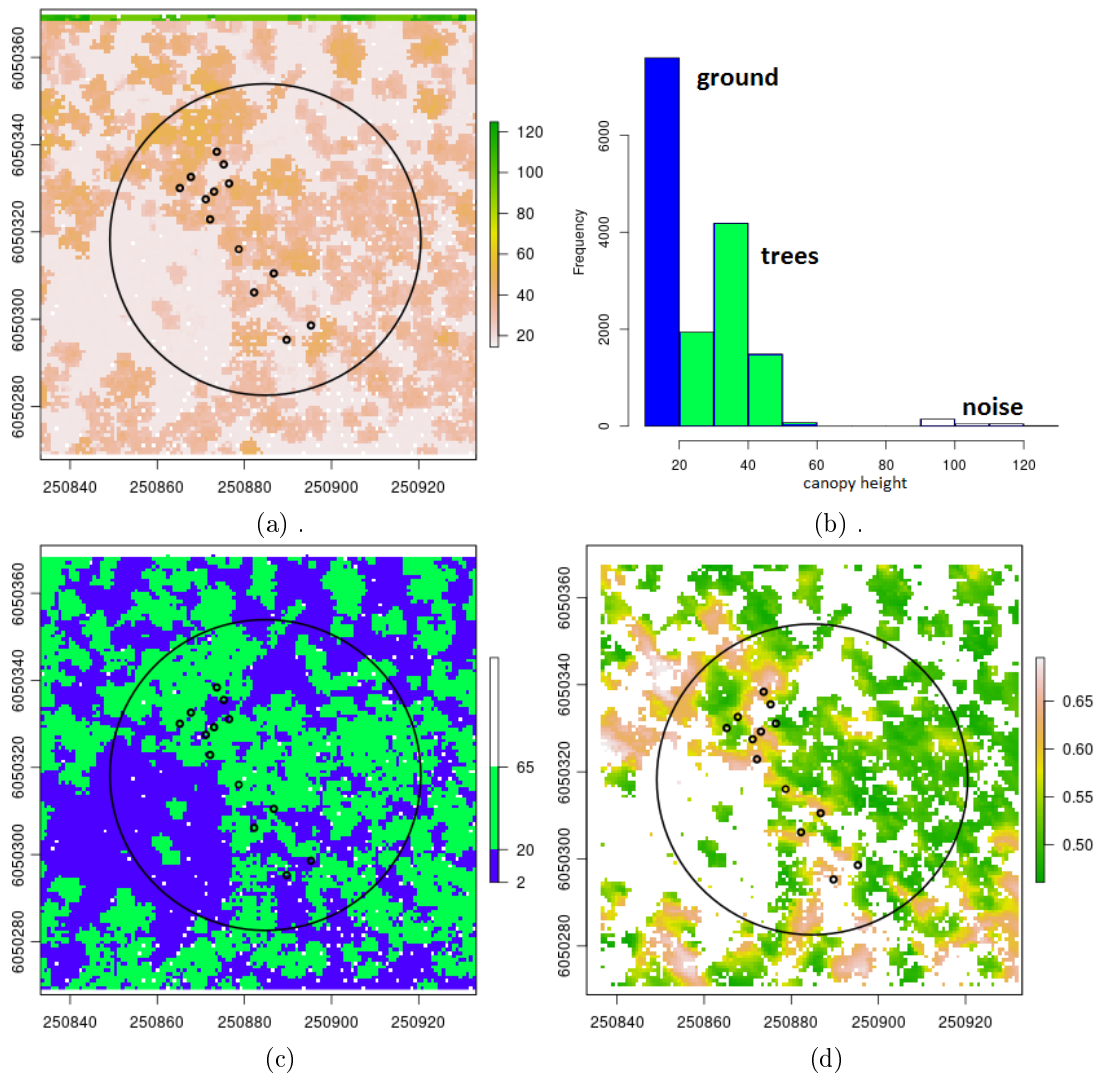


Figure 8-11

8.3.8 Assign dead tree position

for each segment find the middle pixel and assign that as a dead tree

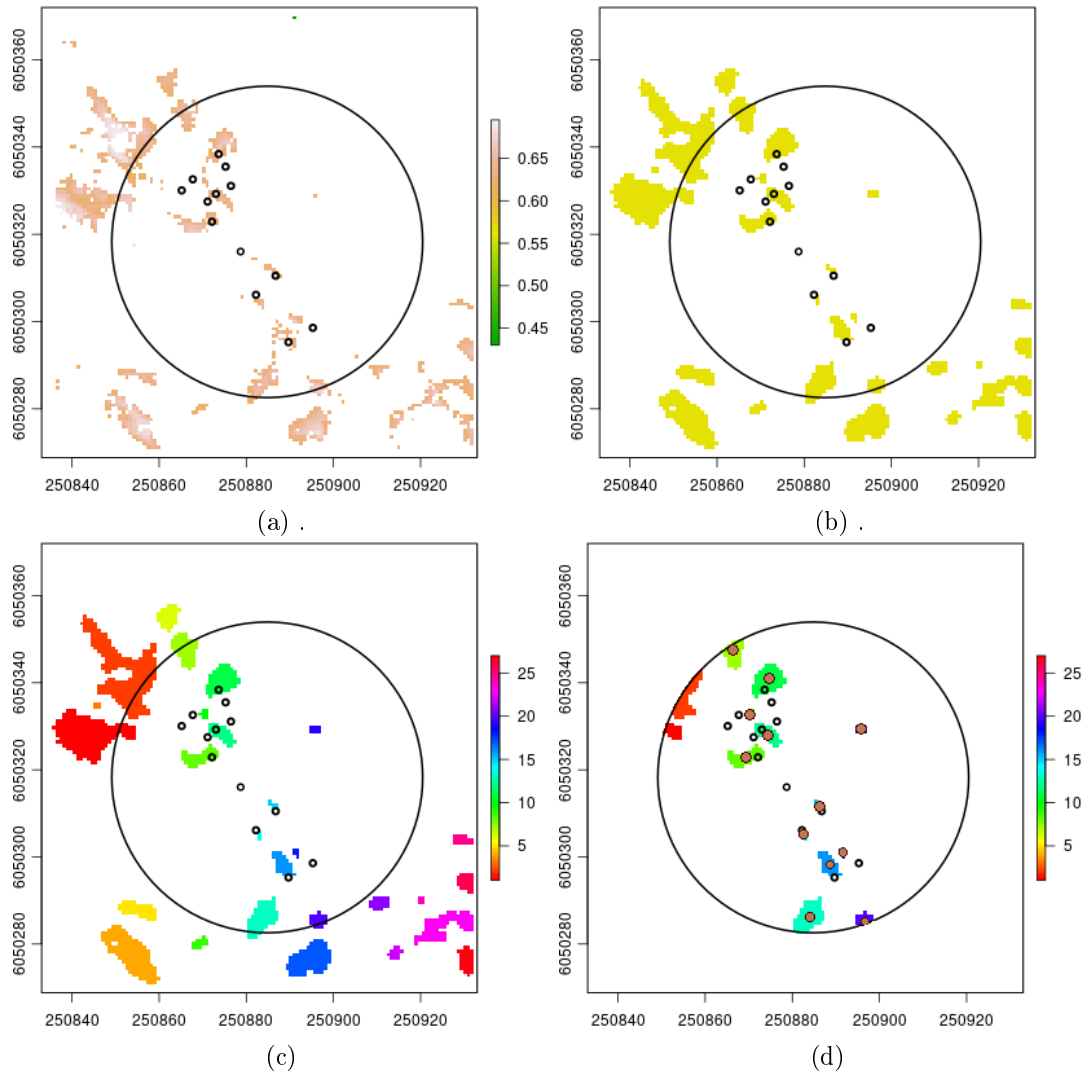


Figure 8-12

8.4 Evaluation

table: Dead tree / Closest Dead Tree id / Distance from Closest ID
precision
recall

8.5 Discussion

Dead tree detection is a difficult task due to the irregular shapes of the trees and different sizes. Here we produced this algorithm (pla pla) which is new because it doesn't need

tree segmentation but has a lot of room for improvement.

Also don't know the accuracy of the tree position and as we can see at some height maps there are places where there are trees according to the fieldplots but the data clearly show that there are not trees

8.6 Future Work

- Manually check and improve position of dead trees using visualisations of the data. In order to improve accuracy of test and evaluating data
- Separate trees from field data according to their height because trees with different heights have different shape properties and the priors used had constant size
- Create priors that have adjustable size according to the height of the tree
- After the seed growth algorithm, check the size of the segments and look into the possibility of merging two segments into one or dividing a segment into multiple sub-segments.
- Test the results when only using dead trees for training data and not alive
- The system is usually confused at the edges of the alive trees. Research on how this could be improved.

Chapter 9

Overall Results

Chapter 10

Conclusions

10.1 Contributions

Bibliography

- [1] T. Elmqvist, C. Folke, M. Nyström, G. Peterson, J. Bengtsson, B. Walker, and J. Norberg, “Response diversity, ecosystem change, and resilience,” *Frontiers in Ecology and the Environment*, vol. 1, no. 9, pp. 488–494, 2003.
- [2] D. U. Hooper, F. S. Chapin Iii, J. J. Ewel, A. Hector, P. Inchausti, S. Lavorel, and B. Schmid, “Effects of biodiversity on ecosystem functioning: a consensus of current knowledge,” *Ecological monographs*, vol. 75, no. 1, pp. 3–35, 2005.
- [3] D. B. Lindenmayer and J. T. Wood, “Long-term patterns in the decay, collapse, and abundance of trees with hollows in the mountain ash (eucalyptus regnans) forests of victoria, southeastern australia,” *Canadian Journal of Forest Research*, vol. 40, no. 1, pp. 48–54, 2010.
- [4] R. L. Goldingay, “Characteristics of tree hollows used by australian birds and bats,” *Wildlife Research*, vol. 36, no. 5, pp. 394–409, 2009.
- [5] P. Gibbons and D. Lindenmayer, *Tree Hollows and Wildlife Conservation in Australia*. CSIRO Publishing, 2002.
- [6] “Animal pests: Poss.” <http://www.doc.govt.nz/conservation/threats-and-impacts/animal-pests/animal-pests-a-z/possums/>. Accessed: 19th of September 2014.
- [7] D. H. DeHayes, P. G. Schaberg, G. J. Hawley, and G. R. Strimbeck, “Acid rain impacts on calcium nutrition and forest health alteration of membrane-associated calcium leads to membrane destabilization and foliar injury in red spruce,” *BioScience*, vol. 49, no. 10, pp. 789–800, 1999.
- [8] J. Holmgren, “Prediction of tree height, basal area and stem volume in forest stands using airborne laser scanningce,” *Scandinavian Journal of Forest Research*, vol. 19, no. 6, pp. 543–553, 2004.

- [9] S. G. Aracil and R. B. A. Herries, D.L, “Evaluation of an additional lidar metric in forest inventory,” *Proceedings of Silvilaser*, 2015.
- [10] M. J. Harper, M. A. McCarthy, R. Van Der Ree, and J. C. Fox, “Overcoming bias in ground-based surveys of hollow-bearing trees using double-sampling,” *Forest Ecology and Management*, vol. 190, no. 2, pp. 291–300, 2004.
- [11] L. Rayner, M. Ellis, and J. E. Taylor, “Double sampling to assess the accuracy of ground-based surveys of tree hollows in eucalypt woodlands,” *Forest Ecology and Management*, vol. 36, no. 3, pp. 252–260, 2011.
- [12] R. B. Smith, *Introduction to Hyperspectral Imaging*. MicroImages, 2014.
- [13] W. Wanger, A. Ullrich, T. Melzer, C. Briese, and K. Kraus, “From single-pulse to ful-waveform airborne laser scanners,” *ISPRS Journal of Photogrammetry and Remote Sensing*, vol. 60, pp. 100–112, 2004.
- [14] A. Wehr and U. Lohr, “Airborne laser scanning - an introduction and overview,” *ISPRS Journal of Photogrammetry and Remote Sensing*, vol. 54, pp. 68–82, 1999.
- [15] C. Mallet and F. Bretar, “Full-waveform topographic lidar: State-of-the-art,” *ISPRS Journal of Photogrammetry and Remote Sensing*, vol. 64, pp. 1–16, 2009.
- [16] K. Anderson, S. Hancock, M. Disney, and K. Gaston, “Is waveform worth it? a comparison of lidar approaches for vegetation and landscape characterization,” *Remote Sensing in Ecology and Conservation*, 2015.
- [17] A. Chauve, C. Mallet, F. Bretar, S. Durrieu, M. Deseilligny, and W. Puech, “Processing full-waveform lidar data: Modelling raw signals,” *International Archives of Photogrammetry, Remote Sensing and Spatial Information Sciences*, 2007.
- [18] *LAS Specification version 1.3-R1*. Bethesda, Maryland: American Society for Photogrammetry and Remote Sensing, 2010.
- [19] M. Warren, *Full Waveform Upgrade*. NERC ARSF wiki, 2012.
- [20] M. J. Sumnall, R. A. Hill, and S. A. Hinsley, “Comparison of small-footprint discrete return and full waveform airborne lidar data for estimating multiple forest variables,” *Remote Sensing of Environment*, vol. 173, pp. 214–223, 2016.
- [21] K. H. R. A. . Z. A. Lehner, H., “Consideration of laser pulse fluctuations and automatic gain control in radiometric calibration of airborne laser scanning data.,” *Proceedings of 6th ISPRS Student Consortium and WG VI/5 Summer School*, 2011.

- [22] I. Korpela, H. O. Ørka, H. V. Hyppä, J., and T. Tokola, “Range and agc normalization in airborne discrete-return lidar intensity data for forest canopies,” vol. 65, no. 4, pp. 369–379, 2010.
- [23] M. Isenburg, *LAStools - efficient tools for LiDAR processing*. rapidlasso.
- [24] M. Warren, B. Taylor, M. Grant, and J. D. Shutler, “Data processing of remorely sensed airborne hyperspectral data using the airborne processing library (apl),” *ScienceDirect, Computers and Geosciences*, vol. 64, 2014.
- [25] M. Isenburg, “Pulsewaves: An open, vendor-neutral, stand-alone, las-compatible full waveform lidar standard.,” 2012.
- [26] A. Persson, U. Soderman, J. Topel, and S. Ahlberg, *Visualisation and Analysis of full-waveform airborne laser scanner data*. V/3 Workshop, Laser scanning 2005, 2005.
- [27] M. Miltiadou, M. A. Warren, M. Grant, and M. Brown, “Alignment of hyperspectral imagery and full-waveform lidar data for visualisation and classification purposes,” *The International Archives of Photogrammetry, Remote Sensing and Spatial Information Sciences*, vol. 40, no. 7, p. 1257, 2015.
- [28] W. Wanger, A. Ullrich, V. Ducic, T. Maizer, and N. Studnicka, “Gaussian decompositions and calibration of a novel small-footprint full-waveform digitising airborne laser scanner,” *ISPRS Journal of Photogrammetry and Remote Sensing*, vol. 60, pp. 100–112, 2006.
- [29] A. Neuenschwander, L. Magruder, and M. Tyler, “Landcover classification of small-footprint full-waveform lidar data,” *Jounal of Applied Remote Sensing*, vol. 3, no. 1, pp. 033544–033544.
- [30] J. Reitberger, P. Krzystek, and U. Stilla, “Analysis of full waveform LiDAR data for tree species classification,” *International Journal of Remote Sensing*, vol. 29, no. 5, pp. 1407–1431, 2008.
- [31] A. Chauve, F. Bretar, S. Durrieu, M. Pierrot-Deseilligny, and W. Puech, “Fullanalyse: A research tool for handling, processing and analysing full-waveform lidar data,” *IEEE International Geoscience and Remote Sensing Symposium*, 2009.
- [32] P. Bunting, J. Armston, D. Clewley, and R. M. Lucas, “Sorted pulse data (spd) library—part ii: A processing framework for lidar data from pulsed laser systems in terrestrial environments,” *Computers & Geosciences*, vol. 56, pp. 207–215, 2013.

- [33] L. Cao, N. Coops, L. Innes, J. Dai, and H. Ruan, “Tree species classification in subtropical forests using small-footprint full-waveform lidar data,” *International Journal of Applied Earth Observation and Geoinformation*, vol. 49, pp. 39–51, 2016.
- [34] S. Hancock, K. Anderson, M. Disney, and K. J. Gaston, “Measurement of fine-spatial-resolution 3d vegetation structure with airborne waveform lidar: Calibration and validation with voxelised terrestrial lidar,” *Remote Sensing of Environment*, vol. 188, pp. 37–50, 2017.
- [35] M. Miltiadou, M. Grant, M. Brown, M. Warren, and E. Carolan, “Reconstruction of a 3d polygon representation from full-wavefrom lidar data,” *RSPSoc Annual Conference 2014, New Sensors for a Changing World*, 2014.
- [36] R. Crippen, “Calculating the vegetation index faster,” *Remote Sensing of Environment*, vol. 34, no. 1, pp. 71–73, 1990.
- [37] R. N. Clark, G. A. Swayze, R. Wise, K. E. Livo, T. Hoefen, R. F. Kokaly, and S. J. Sutley, “Usgs digital spectral library splib06a,” *US Geological Survey, Digital Data Series*, vol. 231, 2007.
- [38] P. Hanrahan, “Ray tracing algebraic surfaces,” *ACM SIGGRAPH Computer Graphics*, vol. 17, no. 3., 1983.
- [39] H. Pfister, J. Harderbergh, J. Knittel, H. Lauer, and L. Seiler, “The volumepro real-time ray-casting system,” *Proceedings of the 26th annual conference on Computer graphics and interactive techniques*, pp. 251–260, 1999.
- [40] J. Nickolls, I. Buck, M. Garland, and K. Skadron, “Scalable parallel programming with cuda,” *Queue*, vol. 6, no. 2, pp. 40–55, 2008.
- [41] C. Crassin, F. Neyret, S. Lefebvre, and E. Eisemann, “Gigavoxels: Ray-guided streaming for efficient and detailed voxel rendering,” *Proceedings of the 2009 symposium on Interactive 3D graphics and games*, pp. 15–22, 2009.
- [42] J. F. Blinn, *A Generalization of Algebraic Surface Drawing*, vol. 1. ACM Transactions on Graphics (TOG).
- [43] A. Pasko and V. Savchenko, *Blending operations for the functionally based constructive geometry*. 1994.

- [44] W. E. Lorensen and H. E. Cline, “Marching cubes: A high resolution 3d surface construction algorithm,” *ACM Siggraph Computer Graphics*, vol. 21, pp. 163–169, 1987.
- [45] M. Levoy, “Volume rendering: Display of surfaces from volume data,” *IEEE Computer Graphics and Applications*, vol. 8, no. 3, pp. 29–37, 1998.
- [46] M. Hadwiger, J. Beyer, W. K. Jeong, and H. Pfister, “Interactive volume exploration of petascale microscopy data streams using visualization-driven virtual memory approach,” *IEEE Transactions on Visualization and Computer Graphics*, 2012.
- [47] S. Laine and T. Karras, “Efficient sparse voxel octrees,” *Visualization and Computer Graphics, IEEE Transactions*, vol. 17, no. 8, pp. 1048–1059, 2011.
- [48] B. Rodrigues de Araujo and J. A. Pires Jorge, *Adaptive polygonization of implicit surfaces*, vol. 29. Science Direct, Computer and Graphics, 2005.
- [49] E. Hartmann, “A marching method for the triangulation of surfaces,” *The Visual computer* 14, no. 14, no. 3, pp. 95–108, 1998.
- [50] C. D. Hansen and P. Hinken, “Massively parallel isosurface extraction,” *Proceedings of the 3rd conference on Visualization '92*, pp. 77–83, 1992.
- [51] C. Galbraith, P. MacMurchy, and B. Wyvill, *BlobTree Trees*. IEEE Computer Graphics International, 2004.
- [52] H. Sutter and A. Alexandrescu, *C++ Coding Standards: 101 Rules, Guidelines, and Best Practices*. United States: Addison-Wesley, 2004.
- [53] J. Wilhelms and A. Van Gelder, “Octrees for faster isosurface generation,” vol. 24, no. 5, 1990.
- [54] W. J. Schaefer, S., “Dual marching cubes: Primal contouring of dual grids,” *Computer Graphics Forum*, vol. 24, no. 2, 2005.
- [55] J. Wilhelms and A. Van Gelder, “Octrees for faster isosurface generation,” *ACM Transactions on Graphics (TOG)*, vol. 11, no. 3, pp. 201–227, 1992.
- [56] S. F. Gibson, “Constrained elastic surface nets: Generating smooth surfaces from binary segmented data,” *International Conference on Medical Image Computing and Computer-Assisted Intervention*, pp. 888–898, 1998.
- [57] B. Chazelle and L. J. Guibas, “Fractional cascading: I. a data structuring technique.,” *Algorithmica*.

- [58] K. Museth, “Vdb: High-resolution sparse volumes with dynamic topology,” *ACM Transactions on Graphics (TOG)*, vol. 32, no. 3, p. 27, 2013.
- [59] M. S. Warren and J. K. Salmon, “A parallel hashed oct-tree n-body algorithm,” *In Proceedings of the 1993 ACM/IEEE conference on Supercomputing*, pp. 12–21, 1993.
- [60] M. Nießner, M. Zollhöfer, S. Izadi, and M. Stamminger, “Real-time 3d reconstruction at scale using voxel hashing,” *ACM Transactions on Graphics (TOG)*, vol. 32, no. 2, p. 169, 2013.
- [61] F. C. Crow, “Summed-area tables for texture mapping,” *ACM Computer Graphics*, vol. 18, no. 3, pp. 207–212, 1984.
- [62] S. Hanan, “Neighbor finding in images represented by octrees,” *Computer Vision, Graphics, and Image Processing*, vol. 46, no. 3, pp. 367–386, 1989.
- [63] G. Schrack, “Finding neighbors of equal size linear quadtrees and octrees in constant time,” *CVGIP: Image Understanding*, vol. 55, no. 3, pp. 221–230, 1992.
- [64] R. Lohner, “Robust, vectorized search algorithms for interpolation on unstructured grids,” *Journal of Computational Physics*, vol. 118, no. 2, pp. 380–387, 1995.
- [65] R. Castro, T. Lewiner, H. Lopes, G. Tavares, and A. Bordignon, “Statistical optimisation of octree searches,” *Computer Graphics Forum*, vol. 27, no. 6, pp. 1557–1566, 2008.
- [66] M. L. Clark, D. A. Roberts, J. J. Ewel, and D. B. Clark, “Estimation of tropical rain forest aboveground biomass with small-footprint lidar and hyperspectral sensors,” *ScienceDirect, Remote Sensing of Environment*, vol. 115.
- [67] J. E. Anderson, L. C. Plourde, M. E. Martin, B. H. Braswell, M. L. Smith, R. O. Dubayah, M. A. H. Dubayah, and J. B. Blair, “Integrating waveform lidar with hyperspectral imagery for inventory of a northern temperate forest,” *Remote Sensing of Environment*, vol. 112, no. 4, pp. 1856–1870, 2008.
- [68] H. Buddenbaum, S. Seeling, and J. Hill, “Fusion of full-waveform lidar and imaging spectroscopy remote sensing data for the characterization of forest stands,” *International Journal of Remote Sensing*, vol. 32, no. 13, pp. 4511–4524, 2013.
- [69] J. Heinzel and B. Koch, “Investigating multiple data sources for tree species classification in temperate forest and use for single tree delineation,” *International*

Journal of Applied Earth Observation and Geoinformation, vol. 18, pp. 101–110, 2012.

- [70] R. G. Congalton, “A review of assessing the accuracy of classifications of remotely sensed data,” *Remote Sensing of Environment*, vol. 37, no. 1.
- [71] J. F. Franklin, H. H. Shugart, and M. E. Harmon, “Tree death as an ecological process,” *BioScience*, vol. 17, no. 8, pp. 550–556, 1987.
- [72] J. Siitonens, “Forest management, coarse woody debris and saprophytic organisms: Fennoscandian boreal forests as an example,” *Ecological bulletins*, pp. 11–41, 2001.
- [73] I. Hanski, “Extinction debt and species credit in boreal forests: modelling the consequences of different approaches to biodiversity conservation,” *Annales Zoologici Fennici*, pp. 271–280, 2000.
- [74] G. Peterson, C. R. Allen, and C. S. Holling, “Ecological resilience, biodiversity, and scale.,” *Ecosystems*, vol. 1, no. 1, pp. 6–18, 1998.
- [75] N. Abrego and I. Salcedo, “How does fungal diversity change based on woody debris type? a case study in northern spain,” *Ekologija*, vol. 57, no. 3, 2011.
- [76] J. N. Stokland and K. H. Larsson, “Legacies from natural forest dynamics: Different effects of forest management on wood-inhabiting fungi in pine and spruce forests,” *Forest Ecology and Management*, vol. 261, no. 11, pp. 1707–1721, 2011.
- [77] D. Lonsdale, M. Pautasso, and O. Holdenrieder, “Wood-decaying fungi in the forest: conservation needs and management options,” *European Journal of Forest Research*, vol. 127, no. 1, pp. 1–22, 2008.
- [78] “List of extinct, threatened and near threatened australian birds,” *Environment Protection and Biodiversity Conservation Act*, 1999.
- [79] Government of Western Australia, “Oaks and wildlife the list of threatened and priority fauna list,” tech. rep., November 2015.
- [80] Y. Kim, Z. Yang, W. B. Cohen, D. Pflugmacher, C. L. Lauver, and J. L. Vankat, “Distinguishing between live and dead standing tree biomass on the north rim of grand canyon national park, usa using small-footprint lidar data.,” *Remote Sensing of Environment*, vol. 113, no. 11, pp. 2499–2510, 2009.
- [81] P. Polewski, W. Yao, M. Heurich, P. Krzystek, and U. Stilla, “Detection of fallen trees in als point clouds using a normalized cut approach trained by simulation,”

ISPRS Journal of Photogrammetry and Remote Sensing, vol. 105, pp. 252–271, 2015.

- [82] W. Mücke, B. Deák, H. M. Schroiff, A., and N. Pfeifer, “Detection of fallen trees in forested areas using small footprint airborne laser scanning data,” *Canadian Journal of Remote Sensing*, vol. 139, no. s1, pp. S32–S40, 2013.
- [83] W. Yao, P. Krzystek, and M. Heurich, “Identifying standing dead trees in forest areas based on 3d single tree detection from full-waveform lidar data,” *ISPRS Annals of the Photogrammetry, Remote Sensing and Spatial Information Sciences*, vol. I-7, pp. 359–364, 2012.
- [84] J. Pasher and D. J. King, “Mapping dead wood distribution in a temperate hard-wood forest using high resolution airborne imagery,” *Forest Ecology and Management*, vol. 258, no. 7, pp. 1536–1548, 2009.
- [85] I. Shendryk, M. Broich, M. G. Tulbure, A. McGrath, D. Keith, and S. V. Alexandrov, “Mapping individual tree health using full-waveform airborne laser scans and imaging spectroscopy: A case study for a floodplain eucalypt forest,” *Remote Sensing of Environment*, vol. 187, pp. 202–217, 2016.
- [86] S. C. Popescu, R. H. Wynne, and R. F. Nelson, “Measuring individual tree crown diameter with lidar and assessing its influence on estimating forest volume and biomass,” *Canadian journal of remote sensing*, vol. 29, no. 5, pp. 564–577, 2003.
- [87] L. Jing, B. Hu, J. Li, and T. Noland, “Automated delineation of individual tree crowns from lidar data by multi-scale analysis and segmentation,” *Photogrammetric Engineering & Remote Sensing*, vol. 78, no. 12, pp. 1275–1284, 2012.
- [88] B. Hu, J. Li, L. Jing, and A. Judah, “Improving the efficiency and accuracy of individual tree crown delineation from high-density lidar data,” *International Journal of Applied Earth Observation and Geoinformation*, vol. 26, pp. 145–15, 2014.
- [89] S. C. Popescu and K. Zhao, “A voxel-based lidar method for estimating crown base height for deciduous and pine trees,” *Remote sensing of environment*, vol. 112, no. 3, pp. 767–781, 2008.
- [90] I. Shendryk, M. Broich, M. G. Tulbure, and S. V. Alexandrov, “Bottom-up delineation of individual trees from full-waveform airborne laser scans in a structurally complex eucalypt forest,” *Remote Sensing of Environment*, vol. 173, pp. 69–83, 2016.

- [91] J. L. Lovell, D. L. B. Jupp, G. J. Newnham, N. C. Coops, and D. S. Culvenor, “Simulation study for finding optimal lidar acquisition parameters for forest height retrieval.,” *Forest Ecology and Management*, vol. 214, no. 1.
- [92] P. Viola and M. Jones, “Rapid object detection using a boosted cascade of simple features,” *Computer Vision and Pattern Recognition*, vol. 1, 2001.
- [93] P. Dong, “Characterization of individual tree crowns using three-dimensional space signatures derived from lidar data.,” *International Journal of Remote Sensing*, vol. 30, no. 24, pp. 6621–6628, 2009.
- [94] J. Kerle, “Collation and review of stem density data and thinning prescriptions for the vegetation communities of new south wales,” 2005.
- [95] N. Wilson and N. C. C. of N.S.W, “The flooded gum trees : land use and management of river red gums in new south wales,” *The Council, Sydney*, 1995.
- [96] E. van Rees, “Trimble’s ax60i and ax80,” *GeoInformatics*, vol. 7, no. 5.
- [97] M. Miltiadou, N. D. F. Campbell, M. Brown, A. S. G., M. Warren, D. Clewley, and M. Grant, “User guide of the 2nd version o dasos,” 2017.
- [98] M. Sumnall, *Assessment of habitat condition and conservation status for lowland British woodland using earth observation techniques*. Bournemouth University: Unpublished PhD thesis, 2013.

Appendix A

DASOS user guide

Appendix B

Case Study: Field Work in New Forest